

Quantum Spin Glass in the Two-Dimensional Disordered Heisenberg Model via Foundation Neural-Network Quantum States

Luciano Loris Viteritti,^{1,*} Riccardo Rende,² Giacomo Bracci Testasecca,^{2,3,†}
Jacopo Niedda,^{4,‡} Roderich Moessner,⁵ Giuseppe Carleo,¹ and Antonello Scardicchio^{4,3,§}

¹*Institute of Physics, École Polytechnique Fédérale de Lausanne (EPFL), CH-1015 Lausanne, Switzerland*

²*SISSA, via Bonomea 265, 34136, Trieste, Italy*

³*INFN, Sezione di Trieste, Via Valerio 2, 34127 Trieste, Italy*

⁴*The Abdus Salam ICTP, Strada Costiera 11, 34151 Trieste, Italy*

⁵*Max Planck Institute for the Physics of Complex Systems, Nöthnitzer Str. 38, 01187 Dresden, Germany*

(Dated: July 8, 2025)

We investigate the two-dimensional frustrated quantum Heisenberg model with bond disorder on nearest-neighbor couplings using the recently introduced Foundation Neural-Network Quantum States framework, which enables accurate and efficient computation of disorder-averaged observables with a single variational optimization. Simulations on large lattices reveal an extended region of the phase diagram where long-range magnetic order vanishes in the thermodynamic limit, while the overlap order parameter, which characterizes quantum spin glass states, remains finite. These findings, supported by a semiclassical analysis based on a large-spin expansion, provide compelling evidence that the spin glass phase is stable against quantum fluctuations, unlike the classical case where it disappears at any finite temperature.

Introduction. Spin glasses have been a fascinating topic of research in both theoretical and experimental physics since their discovery in the 1970s [1, 2]. Since all matter is quantum, when lowering the temperature in a many-body system with quenched disorder, if quantum effects cannot be neglected one speaks of quantum spin glasses (QSG) [3]. Even if quantum fluctuations might represent another equilibration channel, experiments strongly suggest that the spin-glass order persists even at the quantum level, though with a rapid decrease in the characteristic relaxation times and the enhancement of the transition temperature [4, 5]. QSG are a platform to observe the interplay of disorder and frustration in quantum systems, which may lead to parameter chaos [6], the sudden change of ground state configurations when an external parameter is changed by an infinitesimal amount, and possibly to a breakdown of ergodicity (in the form of eigenstate thermalization hypothesis [7, 8]). QSG dynamics can also be a model for the behavior of quantum algorithms [9–13] and, therefore, relevant to a theory of quantum complexity. Recently, glassiness in the quantum realm has been seen also as a way of preventing the system from developing quasiparticle excitations (i.e. to develop non-Fermi liquid behavior) all the way to zero temperature [14, 15]. QSG are also a paradigm for the study of non-equilibrium physics, due to their slow relaxation to equilibrium (aging) [16–18] and to the fact that, in the extreme disorder limit, they prevent equilibration altogether [19].

From a theoretical physicist’s point of view, spin glasses present numerous challenges, which are resilient

to both analytic and numerical treatments. Averaging the observables over the disorder, *i.e.* computing *quenched averages*, analytically requires either the introduction of replicas or of auxiliary fermionic fields. While the latter technique seems more powerful when one wants to describe localization physics in disordered systems [20], the former showed to be useful in devising a mean-field description of the spin glass phase, in terms of Replica Symmetry Breaking [21]. However, neither method allows one to solve for finite-dimensional spin glasses, a situation that has led to controversies regarding the applicability of mean-field theory in low dimensions or the value of the upper and lower critical dimensions of the SG transition [22–26].

From a numerical standpoint, understanding the effects of disorder in low-dimensional frustrated quantum systems remains an open challenge. Quantum Monte Carlo algorithms are hindered by the sign problem, and simulations of disordered systems have mostly been restricted to cases where this limitation is absent, such as the Ising spin glass in a transverse field [27, 28], two-dimensional bipartite antiferromagnets with limited random site or bond dilution [29], or one-dimensional antiferromagnets with ferromagnetic bonds [30, 31]. In general, frustrated disordered magnets in two dimensions can only be tackled using exact diagonalization, which is limited to small system sizes [32–36], or with variational methods. Density Matrix Renormalization Group and related tensor network techniques have proven highly accurate even in two-dimensional disordered systems [37], but face significant limitations compared to their one-dimensional counterparts. These include the need for high-rank tensor structures, or alternatively, restrictions to quasi-one-dimensional geometries using low-rank tensors arranged along a snaked path [38]. Moreover, such approaches often struggle to efficiently implement fully periodic boundary conditions, which are important for

* luciano.viteritti@epfl.ch

† gbraccit@sissa.it

‡ jniedda@ictp.it

§ ascardic@ictp.it

mitigating finite-size effects. Regardless of the computational method employed, one of the main challenges in studying disordered systems lies in the large number of realizations required to precisely compute the disorder-average values of observables.

In this Letter, we investigate the ground-state properties of the two-dimensional quantum Heisenberg model with binary bond disorder on nearest-neighbors couplings. This system is experimentally relevant as a model for the copper-oxygen sheets in lightly doped, insulating high- T_c superconductors. According to Refs. [39–41], localized vacancies on oxygen sites induce effective ferromagnetic couplings between neighboring copper spins, leading to magnetic frustration and possible spin-glass phases. Specifically, using the Foundation Neural-Network Quantum States (FNQS) variational framework introduced in Ref. [42] we circumvent both the sign problem and boundary condition limitations, but most importantly, this method allows the efficient computation of disorder-averaged observables on large lattice sizes at the computational cost of only one variational optimization.

The central result of this study is the identification of an intermediate, non-magnetic phase characterized as a QSG state. A schematic phase diagram of the model summarizing these findings is presented in Fig. 1. To further support our conclusions, we perform a semiclassical analysis based on a large-spin expansion, at the leading order in $1/S$, where S is the spin magnitude. This analysis yields that the classical spin glass (SG) order found at $T = 0$, which is known to be unstable to any $T > 0$ [43, 44], is instead stable against quantum fluctuations. In particular, we find that the leading $1/S$ correction to the spin glass order parameter vanishes in the thermodynamic limit, lending support to the existence of a stable QSG phase at $S = 1/2$, as indicated by our fully quantum numerical simulations.

The model. The two-dimensional Heisenberg model with binary random couplings on an $L \times L$ square lattice is defined by:

$$\hat{H} = \sum_{\langle i,j \rangle} J_{ij} \hat{\mathbf{S}}_i \cdot \hat{\mathbf{S}}_j, \quad (1)$$

where $\hat{\mathbf{S}}_i = (\hat{S}_i^x, \hat{S}_i^y, \hat{S}_i^z)$ is the $S = 1/2$ spin operator at site i and the sum runs only over nearest-neighbor sites, assuming periodic boundary conditions (PBC). The exchange couplings J_{ij} are randomly distributed according to the probability distribution:

$$P(J_{ij}) = (1-p)\delta(J_{ij} + 1) + p\delta(J_{ij} - 1), \quad (2)$$

being $p \in [0, 1]$ the probability to have an antiferromagnetic bond between site i and j . The ground state is well understood in two limiting cases: at $p = 1$, where the model reduces to the antiferromagnetic Heisenberg model, exhibiting long-range Néel order [45, 46], and at $p = 0$, where ferromagnetic order dominates. However,

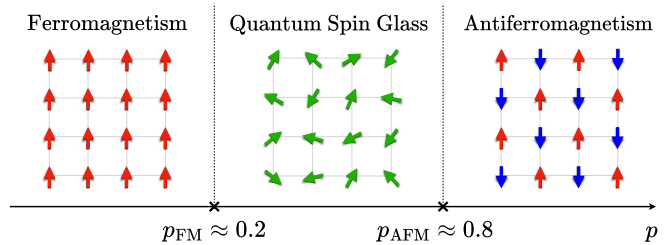


FIG. 1. Ground-state phase diagram of the disordered Heisenberg model [see Eq. (1)] in the thermodynamic limit, as a function of the probability $p \in [0, 1]$ [see Eq. (2)]. Three distinct phases are identified: a ferromagnetic phase for $p \leq p_{\text{FM}} \approx 0.2$, an antiferromagnetic phase for $p \geq p_{\text{AFM}} \approx 0.8$, and an intermediate quantum spin glass phase characterized by the absence of magnetic order and a finite overlap parameter Q (see *Numerical Results* for details). The phase diagram is obtained using the variational approach based on Foundation Neural-Network Quantum States (refer to *Methods*).

for a generic value of $0 < p < 1$, this model is notably challenging to simulate with standard techniques, and in the highly frustrated regime $p \approx 1/2$, the nature of the ground state remains elusive.

Previous studies [32–34] have suggested the possibility of a QSG phase; however, these findings were limited by exact diagonalization results obtained on small 4×4 clusters and are far from compelling. In Ref. [47], square-lattice antiferromagnets were studied at low temperatures on clusters up to 10×10 sites. However, only up to 10% ferromagnetic bonds were considered, limiting access to the spin-glass regime of primary interest in the present work (which we show it appears when the fraction of ferromagnetic bonds exceeds 20%). More recently, a QSG phase has also been proposed in the corresponding one-dimensional model [31], although its nature is still under debate [30]. At the mean field level, a low temperature SG phase has been found on the fully-connected graph with Gaussian distributed couplings in Ref. [48], through a sophisticated dynamical mean field method, which includes replica symmetry breaking. However, as usual, the applicability of mean-field theory to low dimensions can be questioned.

Methods. We adopt the methodology introduced in Ref. [42], in which a variational quantum state $|\psi_\theta(\mathbf{J})\rangle$, parametrized by neural networks and referred to as a Foundation Neural-Network Quantum State (FNQS), is optimized to minimize the disorder-averaged energy:

$$\mathcal{L}(\theta) = \mathbb{E}_{\mathbf{J}} \left[\frac{\langle \psi_\theta(\mathbf{J}) | \hat{H} | \psi_\theta(\mathbf{J}) \rangle}{\langle \psi_\theta(\mathbf{J}) | \psi_\theta(\mathbf{J}) \rangle} \right], \quad (3)$$

where θ are the variational parameters and \mathbf{J} denotes the full set of binary couplings J_{ij} defining the disordered Hamiltonian in Eq. (1). The expectation value $\mathbb{E}_{\mathbf{J}}[\dots]$ in Eq. (3) is approximated by sampling \mathcal{R} disorder

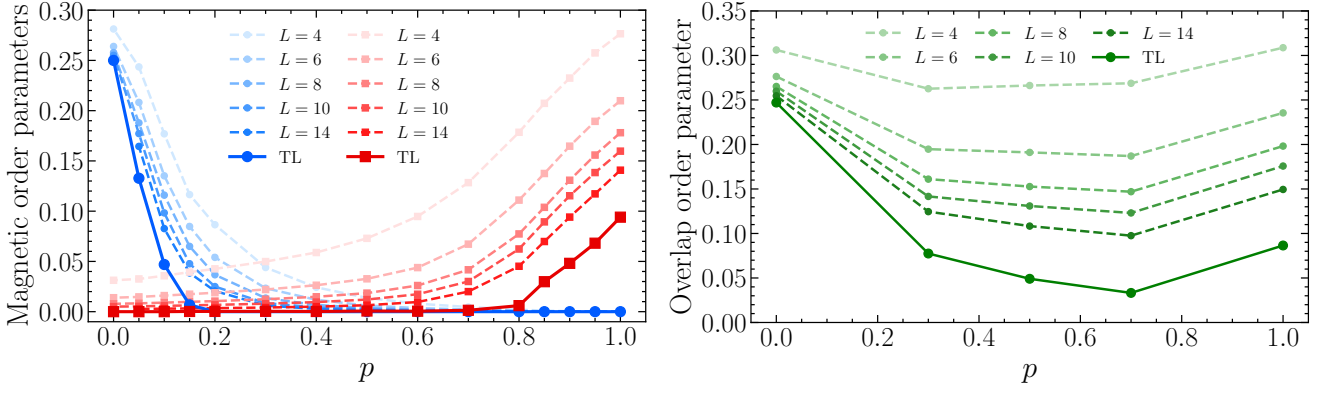


FIG. 2. **Left panel:** Ferromagnetic order parameter $\mathcal{M}_{\text{Ferro}}^2$ (blue circles, dashed lines) and Néel antiferromagnetic order parameter $\mathcal{M}_{\text{Néel}}^2$ (red squares, dashed lines) are shown as a function of the probability p for system sizes ranging from $L = 4$ to $L = 14$. Extrapolated values in the thermodynamic limit (TL), obtained via finite-size scaling in $1/L$ (see *Supplemental Material* for details), are indicated by solid lines connecting the corresponding symbols. **Right panel:** Overlap order parameter Q (green circles, dashed lines) as a function of p for the same system sizes and averaging procedure. Extrapolated TL values are shown as green circles connected by a solid line. Results in both panels are averaged over $\mathcal{R} = 600$ disorder realizations, with $M = 6000$ spin configurations used in the VMC estimates. The FNQS state is optimized via Stochastic Reconfiguration [49–52] for 10^4 steps. The hyperparameters of the ViT architecture are: $n_l = 6$ layers, $h = 14$ attention heads, and embedding dimension $d = 112$ (see Ref. [53] for more details about their role). The total number of variational parameters is $P = 793240$ for $L = 6$ and $P = 988120$ for $L = 14$.

realizations from the distribution $\mathcal{P}(\mathbf{J}) = \prod_{ij} P(J_{ij})$. In the following, for simplicity in the notation, we indicate with $\langle \cdots \rangle_{\mathbf{J}}$ the expectation value on $|\psi_{\theta}(\mathbf{J})\rangle$. For each realization, the variational energy is estimated via Variational Monte Carlo (VMC) [54], using M/\mathcal{R} sampled spin configurations. The key feature of the FNQS approach is that, at no additional computational cost compared to the single-instance case, a variational state can be optimized simultaneously across multiple disorder realizations. This is achieved by making the variational many-body wave function amplitudes $\psi_{\theta}(\sigma|\mathbf{J}) = \langle \sigma | \psi_{\theta}(\mathbf{J}) \rangle$ explicitly dependent on the Hamiltonian couplings \mathbf{J} . Here, σ denotes a spin configuration on a two-dimensional square lattice of linear size L , with local spin variables $\sigma_i = \pm 1$ at each site i , where $i = 1, \dots, N$ with $N = L^2$ the total number of sites. The variational state $\psi_{\theta}(\sigma|\mathbf{J})$ is parametrized with a Vision Transformer (ViT) architecture [51, 53, 55–57], which processes a sequence of n input vectors $\mathbf{x}_1, \dots, \mathbf{x}_n$, each in \mathbb{R}^d , where d is a tunable embedding dimension. In the FNQS framework, the input to the neural network is built to incorporate the Hamiltonian couplings \mathbf{J} as input features of the neural network at the same level as the physical spin configurations σ . Specifically, the spin configuration σ is divided into n non-overlapping patches of size b^2 [53], each embedded into $\mathbb{R}^{d/2}$ through a learnable linear transformation, producing the sequence \mathbf{x}_k^{σ} with $k = 1, \dots, n$. At the same time, each spin σ_i is associated with its two local couplings: the horizontal coupling $J_{i,i+1}$ and the vertical coupling $J_{i,i+L}$, assuming PBC. Using the same patching scheme, the sets of horizontal and vertical

couplings are partitioned into patches and independently embedded into two sequences of vectors, \mathbf{x}_k^h and \mathbf{x}_k^v with $k = 1, \dots, n$, each lying in $\mathbb{R}^{d/4}$. Finally, the input sequence of the model is obtained by concatenating the three embedding vectors at each patch location: $\mathbf{x}_k \equiv \text{Concat}(\mathbf{x}_k^{\sigma}, \mathbf{x}_k^h, \mathbf{x}_k^v) \in \mathbb{R}^d$. This set of n vectors is processed by the ViT wave function, yielding as output a set of another n vectors $\mathbf{y}_k \in \mathbb{R}^d$. The scalar amplitude $\psi_{\theta}(\sigma|\mathbf{J})$ is obtained by summing over the output tokens, $\mathbf{z} = \sum_{k=1}^n \mathbf{y}_k$, and applying a complex-valued two-layer feedforward network with a single output neuron, as detailed in Refs. [42, 53]. This approach enables the efficient evaluation of disorder-averaged observables within a single simulation, substantially improving the scalability of variational methods for disordered systems. Remarkably, the accuracy of the model exhibits minimal degradation with increasing numbers of disorder realizations. Even when trained across hundreds of distinct disorder instances, the FNQS yields observable estimates that closely match those obtained from training on individual realizations with the same architecture (see Section A of the *End Matter*).

Numerical Results. To investigate the possible emergence of a non-magnetic ordered phase at intermediate disorder strengths $0 < p < 1$, we compute the magnetic order parameters characterizing the two limiting cases: ferromagnetic order at $p = 0$ and antiferromagnetic (Néel) order at $p = 1$. The magnetic order parameters are defined as averages over the disorder distribution: $\mathcal{M}_{\text{Ferro}}^2 = \mathbb{E}_{\mathbf{J}} [m_{\text{Ferro}}^2(\mathbf{J})]$ and $\mathcal{M}_{\text{Néel}}^2 = \mathbb{E}_{\mathbf{J}} [m_{\text{Néel}}^2(\mathbf{J})]$, where, for a fixed realization \mathbf{J} , the ferromagnetic order

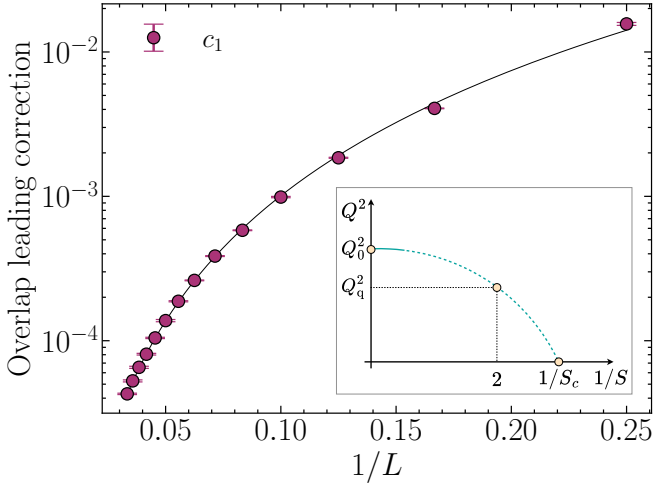


FIG. 3. Size dependence of the leading correction c_1 to the overlap order parameter. The correction vanishes in the thermodynamic limit as $c_1(L) \propto L^{-\alpha}$, with $\alpha \approx 2.9$. **Inset:** Schematic illustration of the expected behavior of the overlap order parameter Q^2 [see Eq. (4)] as a function of $1/S$, where S denotes the spin magnitude. The curve represents the semiclassical expansion, highlighting the vanishing of the leading-order correction in the thermodynamic limit. The value Q_0^2 corresponds to the classical ground state value ($S = \infty$), Q_q^2 corresponds to the quantum result at $S = 1/2$. The critical point $1/S_c$ marks a possible transition from the spin glass phase to a different phase, possibly a spin-fluid state [15] (refer to *Semiclassical Expansion*).

parameter is given by $m_{\text{Ferro}}^2(\mathbf{J}) = C(0, 0; \mathbf{J})/L^2$ while the Néel order parameter is $m_{\text{Néel}}^2(\mathbf{J}) = C(\pi, \pi; \mathbf{J})/L^2$. Both quantities are computed from the spin structure factor, defined as $C(\mathbf{k}; \mathbf{J}) = 1/L^2 \sum_{\mathbf{r}} e^{i\mathbf{k} \cdot \mathbf{r}} \langle \hat{\mathbf{S}}_0 \cdot \hat{\mathbf{S}}_{\mathbf{r}} \rangle_{\mathbf{J}}$. At the two limiting values of the disorder parameter $p = 0$ and $p = 1$, the distribution $\mathcal{P}(\mathbf{J})$ becomes a delta function. Specifically, in the pure ferromagnetic case ($p = 0$), the ground state is fully polarized, and the order parameter can be computed exactly as $\mathcal{M}_{\text{Ferro}}^2 = 1/4 + 1/(2N)$ [58]. In the antiferromagnetic limit ($p = 1$), the model reduces to the standard square-lattice Heisenberg antiferromagnet, for which the Néel order parameter remains finite in the thermodynamic limit, with a known value of $\mathcal{M}_{\text{Néel}} = 0.3070(3)$ [45, 46].

In the interesting intermediate regime $0 < p < 1$, no results are available from other numerical methods aside from exact diagonalization, which we perform up to 6×6 clusters (see Section A of the *End Matter*). In the left panel of Fig. 2, we show the behavior of the magnetic order parameters as a function of p , for system sizes ranging from $L = 4$ to $L = 14$. Each data point corresponds to a single simulation that averages over $\mathcal{R} = 600$ disorder realizations. Then, for each value of p , we perform a finite-size extrapolation in $1/L$ to estimate the magnetic order parameters in the thermodynamic limit (see Section B of the *End Matter* for additional details). Our

extensive numerical calculations identify a region in the phase diagram $0.2 \lesssim p \lesssim 0.8$ where both magnetic order parameters vanish in the thermodynamic limit.

When both magnetic order parameters vanish, it is still possible for the system to exhibit a distinct form of ordering known as glassy order. In a spin glass phase, each spin is aligned along some preferred random direction, which is strongly realization-dependent. To capture the SG order, we look at the long-distance behavior of the correlation function squared, or the *self-overlap*, see for example [59]. We refer to this quantity as the overlap order parameter, denoted here as Q , and defined as:

$$Q^2 = \mathbb{E}_{\mathbf{J}} \left[\frac{1}{L^4} \sum_{\mathbf{r}, \mathbf{r}'} \langle \hat{\mathbf{S}}_{\mathbf{r}} \cdot \hat{\mathbf{S}}_{\mathbf{r}'} \rangle_{\mathbf{J}}^2 \right]. \quad (4)$$

Here, \mathbf{r} and \mathbf{r}' run over all lattice sites, and the value of the overlap is $Q_0^2 = S^2/3$ for a product state of classical, randomly oriented spins of the form $\prod_i |\mathbf{S}_i\rangle$, with \mathbf{S}_i uniformly distributed on the Bloch sphere [60]. Any reduction from the classical value, i.e. $Q^2 < Q_0^2$, means that the fluctuations (quantum or thermal) reduce the persistence of the spins in the chosen, random directions. The right panel of Fig. 2 shows the behavior of Q computed on finite clusters, as a function of the system size. Extrapolating to the thermodynamic limit, we find that Q remains finite throughout the intermediate region $0.2 \lesssim p \lesssim 0.8$, where both magnetic order parameters vanish (see Section B of the *End Matter* for additional details about the extrapolations). Importantly, these findings rule out the presence of disordered states, such as quantum spin liquids or valence bond solids, which are characterized by a vanishing overlap order parameter. Our results provide strong numerical evidence for a QSG phase in this intermediate regime.

Semiclassical analysis. The variational results obtained with the FNQS framework can be checked against a large-spin analysis and computing the leading (in inverse spin length, $1/S$) corrections to the correlation functions and the overlap order parameter. This approach also provides physical insight into the QSG phase. The semiclassical approximation (described in detail in the *Supplemental Material*), is based on the standard Holstein-Primakoff (HP) representation of the spin- S operators. The spin operators can be written in terms of bosonic creation/annihilation operators $\hat{a}_i, \hat{a}_i^\dagger$ satisfying canonical commutation rules $[\hat{a}_i, \hat{a}_j^\dagger] = \delta_{ij}$. The number operator $\hat{a}_i^\dagger \hat{a}_i$ encodes the reduction of the local magnetization compared to the classical Heisenberg vector \mathbf{S}_i . We truncate the HP representation obtained starting from the classical minimum at leading order. This yields a spin-wave correction to the classical energy E_0 , such that the Hamiltonian takes the form $\hat{H} = E_0 + \hat{H}_{\text{SW}}$, with

$$\hat{H}_{\text{SW}} = \sum_{\langle ij \rangle} \hat{a}_i^\dagger A_{ij} \hat{a}_j + \frac{1}{2} \sum_{\langle ij \rangle} \left(\hat{a}_i^\dagger B_{ij} \hat{a}_j^\dagger + \hat{a}_i B_{ij}^* \hat{a}_j \right). \quad (5)$$

The definition of the matrices A, B is given in the *Supplemental Material*. This Hamiltonian does not conserve particle number and must be diagonalized via a Bogoljubov transformation. The ground state spin-spin correlation function yields a $1/S$ correction to the classical spin-spin correlation function:

$$\langle 0 | \hat{\mathbf{S}}_i \cdot \hat{\mathbf{S}}_j | 0 \rangle = \langle \mathbf{S}_i \cdot \mathbf{S}_j \rangle_{\text{cl}} + \frac{1}{S} C_{ij} + O(1/S^2), \quad (6)$$

where $|0\rangle$ represents the Bogoljubov vacuum, i.e. the state in which each spin wave is populated by zero bosons. The final expression of C_{ij} can be found in the *Supplemental Material*. When this expansion is inserted in the definition of Q^2 [see Eq. (4)], it yields $Q^2 = Q_0^2 [1 - c_1/S + O(1/S^2)]$ with $Q_0^2 = S^2/3$ the classical result at $T = 0$. In Fig. 3 the results of the numerical analysis of the spin wave Hamiltonian are presented. Specifically, we show that the leading correction c_1 to the overlap order parameter vanishes in the thermodynamic limit. This validates the results obtained with the FNQS framework, directly discarding the scenario where arbitrarily small quantum fluctuations destroy the spin glass order and moving any correction to $O(1/S^2)$. However, this of course does not exclude the possibility of a critical spin length $\infty > S_c > 1/2$ below which SG order gives in to some competing state with $Q^2 = 0$ (see inset of Fig. 3). The semiclassical analysis also provides a physical picture for the vanishing of this correction. In particular, one observes that all the Bogoljubov modes are spatially localized (with localization length that diverges as their frequency $\omega \rightarrow 0$). In this way, the corrections to Q^2 , which come from long-distance physics, vanish so that the classical SG ordered solution is stable, at large distances, to quantum fluctuations. A detailed analysis of this phenomenon will be presented in a future publication.

Conclusions. We explored the phase diagram of the two-dimensional Heisenberg model with binary disorder on the nearest-neighbor couplings, presenting compelling evidence for a quantum spin glass phase in the thermodynamic limit. Methodologically, we employed a novel variational framework based on FNQS [42], which proves particularly effective for disordered quantum systems. Unlike conventional approaches, FNQS mitigate the high computational cost associated with averaging over many disorder realizations. We validated the numerical result by performing a semiclassical expansion around the classical minimum energy configuration. Among future directions to be explored, there is the numerical characterization of the excitations on top of the QSG state. In particular, if one observes a non-Fermi liquid behavior, from the semiclassical analysis this would correspond to the relevance of the interaction among the Bogoljubov waves. The same aspect could also be investigated analytically, although an analysis of interacting, disordered bosons is notoriously difficult, and few techniques exist for the scope (see for example Ref. [61]). This is clearly

beyond the scope of this paper and is left for future work.

ACKNOWLEDGMENTS

We thank A. Laio, F. Becca, S. Sachdev, and G. Parisi for useful discussions. R.R. and L.L.V. acknowledge the CINECA award under the ISCRA initiative for the availability of high-performance computing resources and support. The work of A.S. and J.N. was funded by the European Union–NextGenerationEU under the project NRRP Project “National Quantum Science and Technology Institute” — NQSTI, Award Number: PE00000023, Concession Decree No. 1564 of 11.10.2022 adopted by the Italian Ministry of Research, CUP J97G22000390007. This work was in part supported by the Deutsche Forschungsgemeinschaft under grants SFB 1143 (project-id 247310070) and the cluster of excellence ct.qmat (EXC 2147, project-id 390858490). This work was supported by the Swiss National Science Foundation under Grant No. 200021_200336. This research was also supported by SE-FRI through Grant No. MB22.00051 (NEQS - Neural Quantum Simulation).

END MATTER

A. Comparison with Exact Diagonalization

In Fig. 4, we assess the accuracy of the FNQS in reproducing the exact spin-spin correlations for a representative disorder realization with $p = 0.7$ on a 6×6 cluster, the largest system size for which exact results via the Lanczos algorithm are feasible. We compare the exact calculations (blue empty circles) with those obtained from a Neural-Network Quantum State (NQS) [62, 63] parameterized with a ViT architecture [53] optimized on this specific realization (green circles), and from a FNQS trained on $\mathcal{R} = 600$ independent disorder realizations (orange diamonds), then evaluated on the same realization. Notably, the two variational approaches have the same computational cost and yield very similar results, yet the FNQS represents a more general state optimized across many disorder realizations. The inset displays the corresponding spin structure factor along a path connecting $\mathbf{k} = (0, 0)$ and $\mathbf{k} = (\pi, \pi)$, which are related to ferromagnetic and antiferromagnetic order, respectively (see *Numerical Results*). The excellent agreement with the exact data highlights the ability of the FNQS to learn the ground state of each single disorder realization with the same accuracy as a neural network trained specifically on that realization.

B. Finite-Size Extrapolations to the Thermodynamic Limit

In this section, we present the finite-size extrapolations of the three relevant order parameters: the antiferromagnetic order parameter $\mathcal{M}_{\text{Néel}}^2$, the ferromagnetic order parameter $\mathcal{M}_{\text{Ferro}}^2$, and the overlap order parameter Q (see *Numerical Results* for their definitions). The extrapolations are shown as a function of inverse system size $1/L$ for system sizes ranging from $L = 4$ to $L = 14$. Each value of the order parameters is obtained by averaging over $\mathcal{R} = 600$ disorder realizations.

In the left panel of Fig. 5, we display the behavior of $\mathcal{M}_{\text{Néel}}^2$ for $p \in [0.4, 1.0]$. Notably, for $p_{\text{AFM}} \approx 0.8$, the extrapolated value vanishes in the thermodynamic limit, indicating the disappearance of antiferromagnetic long-range order. Additionally, we benchmark the variational results against Quantum Monte Carlo data for the unfrustrated case $p = 1$, finding excellent agreement both at finite sizes and in the thermodynamic limit.

The central panel of Fig. 5 shows the extrapolation of the ferromagnetic order parameter $\mathcal{M}_{\text{Ferro}}^2$ for $p \in [0.0, 0.3]$. Here, for $p_{\text{FM}} \approx 0.2$, the extrapolated value also vanishes, signaling the suppression of ferromagnetic order. For $p = 0$, we compare the variational results with the exact analytical prediction available for this limit (see *Numerical Results*), again observing very good agreement.

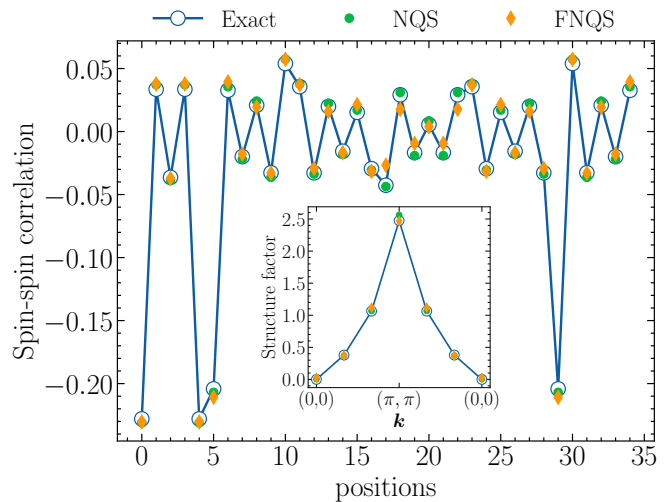


FIG. 4. Spin-spin correlation for a disorder realization with $p = 0.7$ on a 6×6 cluster. For visualization, the two-dimensional lattice is unrolled using the row-major convention. Exact diagonalization results (blue empty circles) are compared with variational calculations: a NQS optimized on the specific disorder realization (green circles) and a FNQS trained on $\mathcal{R} = 600$ disorder realizations (orange diamonds). The inset displays the corresponding structure factor along a path connecting $\mathbf{k} = (0, 0)$ and $\mathbf{k} = (\pi, \pi)$. The neural network hyperparameters are the same as those used in Fig. 2.

Finally, the right panel of Fig. 5 reports the behavior of the overlap parameter Q . For the limiting cases $p = 0$ and $p = 1$, we compare the extrapolated values of Q with the corresponding magnetic order parameters, confirming consistency between the different observables. We also show the extrapolation of Q for intermediate values $p = 0.3, 0.5$, and 0.7 , where both magnetic orders vanish in the thermodynamic limit. In contrast to the magnetic order parameters, Q remains finite, suggesting the presence of a QSG phase in this parameter regime.

C. Self-Averaging and Distribution of Order Parameters

In disordered systems, a central requirement for the validity of statistical predictions is the *self-averaging* property of physical observables. An observable is said to be self-averaging if its fluctuations across different disorder realizations vanish in the thermodynamic limit. This implies that ensemble-averaged quantities become representative of individual realizations as the system size increases. In Fig. 6 we analyze the distributions of the relevant order parameters, namely, the antiferromagnetic order parameter $\mathcal{M}_{\text{Néel}}^2$ (left panel), the ferromagnetic order parameter $\mathcal{M}_{\text{ferro}}^2$ (central panel), and the square of overlap Q^2 (right panel), computed over $\mathcal{R} = 600$ independent disorder realizations. The width of these distri-

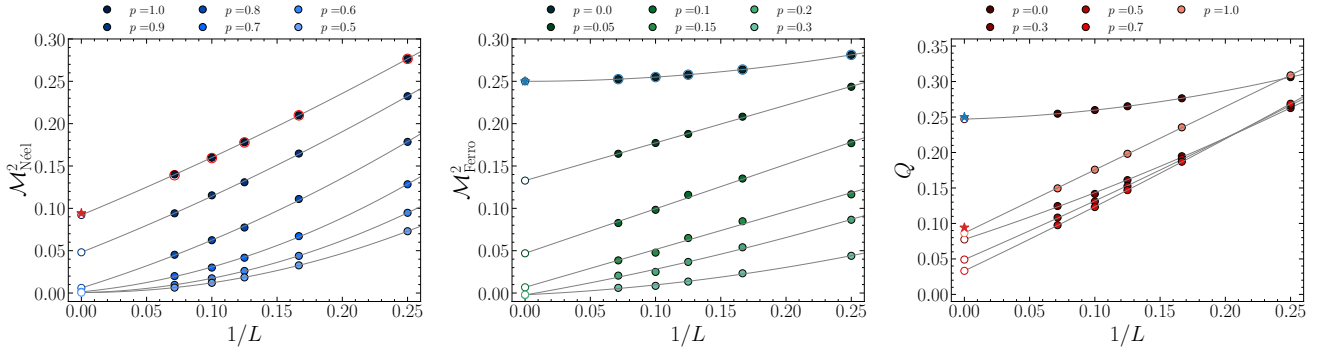


FIG. 5. Finite-size extrapolations of the order parameters as a function of $1/L$: the antiferromagnetic $\mathcal{M}_{\text{Néel}}^2$ (left panel), ferromagnetic $\mathcal{M}_{\text{Ferro}}^2$ (central panel), and overlap Q (right panel) order parameters, averaged over $\mathcal{R} = 600$ disorder realizations for system sizes ranging from $L = 4$ to 14. The data for $L = 4$ are obtained with exact diagonalization techniques. In the left panel, numerically exact Quantum Monte Carlo results for $p = 1.0$ are shown for finite sizes (red empty circles) and thermodynamic limit (red star). In the central panel, analytic results for $p = 0.0$ are shown for finite sizes (blue empty circles) and thermodynamic limit (blue star). In the right panel, thermodynamic-limit values of the Néel (red star) and ferromagnetic (blue star) order parameters are shown for comparison with the overlap Q at $p = 1.0$ and $p = 0.0$, respectively.

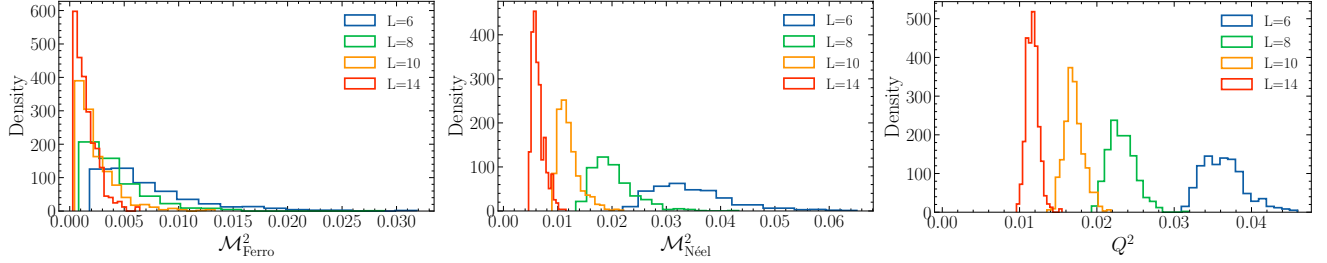


FIG. 6. Distributions of the order parameters $\mathcal{M}_{\text{Ferro}}^2$ (left panel), $\mathcal{M}_{\text{Néel}}^2$ (central panel), and Q^2 (right panel) for $p = 0.5$, considering system sizes ranging from $L = 6$ to $L = 14$. Each distribution is computed using $\mathcal{R} = 600$ independent disorder realizations.

butions systematically decreases with increasing system size L , providing strong evidence of self-averaging.

We emphasize that this property is not only fundamental from a theoretical standpoint but also has important computational implications in our variational approach. In the FNQS framework, a single variational wave function is optimized simultaneously across many disorder realizations. The efficiency and accuracy of this global optimization strategy improve with system size in a self-averaging model: as the fluctuations between different realizations diminish, the structure of the ground states becomes more similar across samples. Consequently, the variational state is able to effectively capture the common features of the ground states in the disordered ensemble.

-
- [1] S. F. Edwards and P. W. Anderson, Theory of spin glasses, *Journal of Physics F: Metal Physics* **5**, 965 (1975).
- [2] J. A. Mydosh, *Spin Glasses: an Experimental Introduction* (CRC Press, 1993).
- [3] L. Cugliandolo and M. Mueller, Quantum glasses, in *Spin Glass Theory and Far Beyond. Replica Symmetry Breaking After 40 Years*, edited by P. Charbonneau, E. Marinari, M. Mézard, G. Parisi, F. Ricci-Tersenghi, G. Sincuro, and F. Zamponi (World Scientific Connect, 2023) Chap. 18.
- [4] W. Wu, B. Ellman, T. F. Rosenbaum, G. Aeppli, and D. H. Reich, From classical to quantum glass, *Phys. Rev. Lett.* **67**, 2076 (1991).
- [5] W. Wu, D. Bitko, T. F. Rosenbaum, and G. Aeppli, Quenching of the nonlinear susceptibility at a $t=0$ spin glass transition, *Phys. Rev. Lett.* **71**, 1919 (1993).
- [6] M. Baity-Jesi, E. Calore, A. Cruz, L. A. Fernandez, J. M. Gil-Narvion, I. Gonzalez-Adalid Pmartin, A. Gordillo-Guerrero, D. Iñiguez, A. Maiorano, E. Marinari, V. Martin-Mayor, J. Moreno-Gordo, A. Muñoz-Sudupe, D. Navarro, I. Paga, G. Parisi, S. Perez-Gaviro, F. Ricci-Tersenghi, J. J. Ruiz-Lorenzo, S. F. Schifano, B. Seoane, A. Tarancon, R. Tripiccion, and D. Yllanes, Temperature chaos is present in off-equilibrium spin-glass dynamics, *Communications Physics* **4**, 74 (2021).
- [7] M. Srednicki, Chaos and quantum thermalization, *Physical review e* **50**, 888 (1994).
- [8] J. M. Deutsch, Eigenstate thermalization hypothesis, *Reports on Progress in Physics* **81**, 082001 (2018).
- [9] G. E. Santoro, R. Martoňák, E. Tosatti, and R. Car, Theory of quantum annealing of an Ising spin glass, *Science* **295**, 2427 (2002), <https://www.science.org/doi/pdf/10.1126/science.1068774>.
- [10] C. Laumann, R. Moessner, and A. Scardicchio, Quantum adiabatic algorithm and scaling of gaps at first-order quantum phase transitions, *Physical review letters* **109**, 030502 (2012).
- [11] Quantum annealing: The fastest route to quantum computation?, *The European Physical Journal Special Topics* **224**, 75 (2015).
- [12] V. Martin-Mayor and I. Hen, Unraveling quantum annealers using classical hardness, *Scientific Reports* **5**, 15324 (2015).
- [13] H. G. Katzgraber, F. Hamze, Z. Zhu, A. J. Ochoa, and H. Munoz-Bauza, Seeking quantum speedup through spin glasses: The good, the bad, and the ugly, *Phys. Rev. X* **5**, 031026 (2015).
- [14] J. Maldacena and D. Stanford, Remarks on the Sachdev-Ye-Kitaev model, *Physical Review D* **94**, 106002 (2016).
- [15] S. Sachdev and J. Ye, Gapless spin-fluid ground state in a random quantum Heisenberg magnet, *Physical review letters* **70**, 3339 (1993).
- [16] L. F. Cugliandolo and G. Lozano, Real-time nonequilibrium dynamics of quantum glassy systems, *Phys. Rev. B* **59**, 915 (1999).
- [17] M. P. Kennett, C. Chamon, and J. Ye, Aging dynamics of quantum spin glasses of rotors, *Phys. Rev. B* **64**, 224408 (2001).
- [18] M. P. Kennett and C. Chamon, Time reparametrization group and the long time behavior in quantum glassy systems, *Phys. Rev. Lett.* **86**, 1622 (2001).
- [19] P. Sierant, M. Lewenstein, A. Scardicchio, L. Vidmar, and J. Zakrzewski, Many-body localization in the age of classical computing, *Reports on Progress in Physics* **88**, 026502 (2025).
- [20] K. Efetov, *Supersymmetry in Disorder and Chaos* (Cambridge University Press, 1996).
- [21] M. Mézard, G. Parisi, and M. A. Virasoro, *Spin glass theory and beyond: An Introduction to the Replica Method and Its Applications*, Vol. 9 (World Scientific Publishing Company, 1987).
- [22] M. A. Moore, The stability of the replica-symmetric state in finite-dimensional spin glasses, *Journal of Physics A: Mathematical and General* **38**, L783 (2005).
- [23] C. D. Dominicis and I. Giardin, *Random Fields and Spin Glasses: a Field Theory Approach* (Cambridge University Press, Hardback, 2006).
- [24] M. A. Moore and A. J. Bray, Disappearance of the de Almeida-thouless line in six dimensions, *Phys. Rev. B* **83**, 224408 (2011).
- [25] J. J. Ruiz-Lorenzo, Nature of the Spin Glass Phase in Finite Dimensional (Ising) Spin Glasses, in *Order, Disorder and Criticality. Advanced Problems of Phase Transition Theory. Volume 6*, edited by Y. Holovatch (World Scientific Connect, 2020) Chap. 1.
- [26] M. C. Angelini, C. Lucibello, G. Parisi, G. Perrupato, F. Ricci-Tersenghi, and T. Rizzo, Unexpected upper critical dimension for spin glass models in a field predicted by the loop expansion around the Bethe solution at zero temperature, *Phys. Rev. Lett.* **128**, 075702 (2022).
- [27] J. Choi and S. K. Baek, Finite-size scaling analysis of the two-dimensional random transverse-field Ising ferromagnet, *Phys. Rev. B* **108**, 144204 (2023).
- [28] C. Krämer, J. A. Koziol, A. Langheld, M. Hörmann, and K. P. Schmidt, Quantum-critical properties of the one- and two-dimensional random transverse-field Ising model from large-scale quantum monte carlo simulations, *SciPost Physics* **17**, 10.21468/scipostphys.17.2.061 (2024).
- [29] A. W. Sandvik, Classical percolation transition in the diluted two-dimensional $s = \frac{1}{2}$ Heisenberg antiferromagnet, *Phys. Rev. B* **66**, 024418 (2002).
- [30] S. Li, H. Shao, and A. W. Sandvik, Ground state of the $s = 1/2$ Heisenberg spin chain with random ferromagnetic and antiferromagnetic couplings, *Phys. Rev. Lett.* **134**, 086501 (2025).
- [31] M. Fava, J. L. Jacobsen, and A. Nahum, Heisenberg spin chain with random-sign couplings, *Proceedings of the National Academy of Sciences* **121**, e2401292121 (2024), <https://www.pnas.org/doi/pdf/10.1073/pnas.2401292121>.
- [32] J. Oitmaa and O. P. Sushkov, Two-dimensional randomly frustrated spin-1/2 Heisenberg model., *Physical review letters* **87**, 167206 (2001).
- [33] L. Arrachea and M. J. Rozenberg, Dynamical response of quantum spin-glass models at $T = 0$, *Phys. Rev. Lett.* **86**, 5172 (2001).
- [34] J. P. Rodriguez, J. Bonča, and J. Ferrer, Random frustration in a two-dimensional spin-1/2 Heisenberg antiferromagnet, *Phys. Rev. B* **51**, 3616 (1995).
- [35] K. Uematsu and H. Kawamura, Randomness-induced quantum spin liquid behavior in the $s = \frac{1}{2}$ random $J_1 - J_2$ Heisenberg antiferromagnet on the square lattice, *Phys.*

- Rev. B **98**, 134427 (2018).
- [36] D. Wu, F. Yang, and G. Carleo, [Unveiling non-magnetic phase and many-body entanglement in two-dimensional random quantum magnets \$\text{Sr}_2\text{CuTe}_{1-x}\text{W}_x\text{O}_6\$](#) (2024), [arXiv:2407.05917 \[cond-mat.str-el\]](#).
 - [37] H.-D. Ren, T.-Y. Xiong, H.-Q. Wu, D. N. Sheng, and S.-S. Gong, Characterizing random-singlet state in two-dimensional frustrated quantum magnets and implications for the double perovskite $\text{Sr}_2\text{CuTe}_{1-x}\text{W}_x\text{O}_6$, [Phys. Rev. B](#) **107**, L020407 (2023).
 - [38] E. Stoudenmire and S. R. White, Studying two-dimensional systems with the density matrix renormalization group, [Annual Review of Condensed Matter Physics](#) **3**, 111–128 (2012).
 - [39] A. Aharony, R. J. Birgeneau, A. Coniglio, M. A. Kastner, and H. E. Stanley, Magnetic phase diagram and magnetic pairing in doped La_2CuO_4 , [Phys. Rev. Lett.](#) **60**, 1330 (1988).
 - [40] A. Aharony, R. Birgeneau, A. Coniglio, M. Kastner, and H. Stanley, Magnetic phases and possible magnetic pairing in doped lanthanum cuprate, [Physica C: Superconductivity](#) **153–155**, 1211 (1988), proceedings of the International Conference on High Temperature Superconductors and Materials and Mechanisms of Superconductivity Part II.
 - [41] M. Frachet, I. Vinograd, R. Zhou, S. Benhabib, S. Wu, H. Mayaffre, S. Krämer, S. K. Ramakrishna, A. P. Reyes, J. Debray, T. Kurosawa, N. Momono, M. Oda, S. Komiyama, S. Ono, M. Horio, J. Chang, C. Proust, D. LeBoeuf, and M.-H. Julien, Hidden magnetism at the pseudogap critical point of a cuprate superconductor, [Nature Physics](#) **16**, 1064–1068 (2020).
 - [42] R. Rende, L. L. Viteritti, F. Becca, A. Scardicchio, A. Laio, and G. Carleo, [Foundation neural-network quantum states](#) (2025), [arXiv:2502.09488 \[quant-ph\]](#).
 - [43] J. F. Fernandez, Isotropic Heisenberg spin-glass order in two dimensions, [Journal of Physics C: Solid State Physics](#) **10**, L441 (1977).
 - [44] H. Kawamura and H. Yonehara, Ordering of the Heisenberg spin glass in two dimensions, [Journal of Physics A: Mathematical and General](#) **36**, 10867 (2003).
 - [45] M. Calandra Buonauro and S. Sorella, Numerical study of the two-dimensional Heisenberg model using a green function monte carlo technique with a fixed number of walkers, [Phys. Rev. B](#) **57**, 11446 (1998).
 - [46] A. W. Sandvik, Finite-size scaling of the ground-state parameters of the two-dimensional Heisenberg model, [Phys. Rev. B](#) **56**, 11678 (1997).
 - [47] A. W. Sandvik, Numerical study of a two-dimensional quantum antiferromagnet with random ferromagnetic bonds, [Phys. Rev. B](#) **50**, 15803 (1994).
 - [48] N. Kavokine, M. Müller, A. Georges, and O. Parcollet, Exact numerical solution of the fully connected classical and quantum Heisenberg spin glass, [Physical Review Letters](#) **133**, 016501 (2024).
 - [49] S. Sorella, Green function monte carlo with stochastic reconfiguration, [Phys. Rev. Lett.](#) **80**, 4558 (1998).
 - [50] S. Sorella, Wave function optimization in the variational monte carlo method, [Phys. Rev. B](#) **71**, 241103 (2005).
 - [51] R. Rende, L. L. Viteritti, L. Bardone, F. Becca, and S. Goldt, A simple linear algebra identity to optimize large-scale neural network quantum states, [Communications Physics](#) **7**, 10.1038/s42005-024-01732-4 (2024).
 - [52] A. Chen and M. Heyl, Empowering deep neural quantum states through efficient optimization, [Nature Physics](#) **20**, 1476 (2024).
 - [53] L. L. Viteritti, R. Rende, A. Parola, S. Goldt, and F. Becca, Transformer wave function for two dimensional frustrated magnets: Emergence of a spin-liquid phase in the shastry-sutherland model, [Phys. Rev. B](#) **111**, 134411 (2025).
 - [54] F. Becca and S. Sorella, [Quantum Monte Carlo Approaches for Correlated Systems](#) (Cambridge University Press, 2017).
 - [55] L. L. Viteritti, R. Rende, and F. Becca, Transformer variational wave functions for frustrated quantum spin systems, [Phys. Rev. Lett.](#) **130**, 236401 (2023).
 - [56] R. Rende, S. Goldt, F. Becca, and L. L. Viteritti, Fine-tuning neural network quantum states, [Phys. Rev. Res.](#) **6**, 043280 (2024).
 - [57] K. Sprague and S. Czischek, Variational monte carlo with large patched transformers, [Communications Physics](#) **7**, 90 (2024).
 - [58] By definition, $C(0,0) = \langle \hat{S}^2 \rangle$, where \hat{S} is the total spin operator. For a fully polarized state $\langle \hat{S}^2 \rangle = S(S+1) = N/2(N/2+1)$, from which the order parameter follows.
 - [59] M. Baity-Jesi and G. Parisi, Inherent structures in m-component spin glasses, [Physical Review B](#) **91**, 134203 (2015).
 - [60] In fact, $\frac{1}{L^4} \sum_{i,j} \sum_{\alpha,\beta} S_i^\alpha S_j^\alpha S_i^\beta S_j^\beta = S^2 \sum_{\alpha,\beta} \frac{1}{3} \delta_{\alpha\beta} \frac{1}{3} \delta_{\alpha\beta} = S^2/3$.
 - [61] T. Giamarchi and H. J. Schulz, Anderson localization and interactions in one-dimensional metals, [Physical Review B](#) **37**, 325 (1988).
 - [62] G. Carleo and M. Troyer, Solving the quantum many-body problem with artificial neural networks, [Science](#) **355**, 602 (2017).
 - [63] H. Lange, A. Van de Walle, A. Abedinnia, and A. Bohrdt, From architectures to applications: a review of neural quantum states, [Quantum Science and Technology](#) **9**, 040501 (2024).

Supplemental Material of Quantum Spin Glass in the Two-Dimensional Disordered Heisenberg Model via Foundation Neural-Network Quantum States

The semiclassical expansion has proven to be an efficient way to capture properties of quantum systems, being able to predict, for example, the difference between the quadratic and linear dispersion relation in one-dimensional ferromagnetic/antiferromagnetic spin 1/2 chains [1]. It relies on the Holstein-Primakoff (HP) mapping of a spin S operator onto bosonic variables, which at the leading order in the classical limit $S \rightarrow \infty$, $\hbar \rightarrow 0$ simplifies to a quadratic bosonic problem. In the following, we present the derivation of the procedure that allows for the computation of the quantum correction to the SG order parameter discussed in the main text (see *Semiclassical Expansion*).

The procedure can be divided into two steps: first, we find the classical ground state for a given coupling realization; then, we build up the HP machinery, which will produce a quadratic Hamiltonian, describing quantum fluctuations around the classical configuration of minimal energy. The classical model is defined as

$$E_{cl} = \sum_{\langle i,j \rangle} J_{ij} \mathbf{S}_i \cdot \mathbf{S}_j, \quad (1)$$

where \mathbf{S}_i is an $O(3)$ vector and $J_{ij} = \pm 1$ a random sign nearest neighbors coupling term. The model is known to have a SG phase in $d = 3$ on the cubic lattice [2], while in $d = 2$, SG order is only found at $T = 0$ [3, 4].

To find the ground state, we resort to a greedy single-spin update optimization algorithm, presented e.g. in Ref. [5]. For a given initial condition, the algorithm performs a deterministic energy minimization procedure, which crucially depends on the number of restarts: in general, for large system sizes L and a reasonable number of restarts N_r , finding the global minimum is not guaranteed, though its occurrence is exponentially larger than the local minima. However, this is not annoying for our purposes, since we have checked that the outcome of the semiclassical computation does not depend on whether the global or a *low energy* local minimum has been selected. This is not surprising, since the semiclassical expansion is a non-perturbative computation that depends only on local quantities (the Hessian matrix of the minimum).

In order to prove the statistical equivalence between the semiclassical expansion over different minima, we consider the distribution of the quantum correction to the SG order parameter Q . We study the case of $L = 8$, where we are sure to find the true ground state with $N_r = 10L^2$ restarts of the algorithm. In Fig. 1 we show the probability distributions of the overlap correction computed in the global minimum and in the first local minima. The Kolmogorov-Smirnov hypothesis test confirms quantitatively the statistical equivalence of the distributions.

THE HOLSTEIN-PRIMAKOFF TRANSFORMATION

A spin S operator can be mapped onto a set of bosonic variables via the HP transformation defined as

$$\hat{S}_i^z = S - \hat{a}_i^\dagger \hat{a}_i, \quad \hat{S}_i^+ = \sqrt{2S - \hat{a}_i^\dagger \hat{a}_i} \hat{a}_i, \quad \hat{S}_i^- = \hat{a}_i^\dagger \sqrt{2S - \hat{a}_i^\dagger \hat{a}_i}, \quad (2)$$

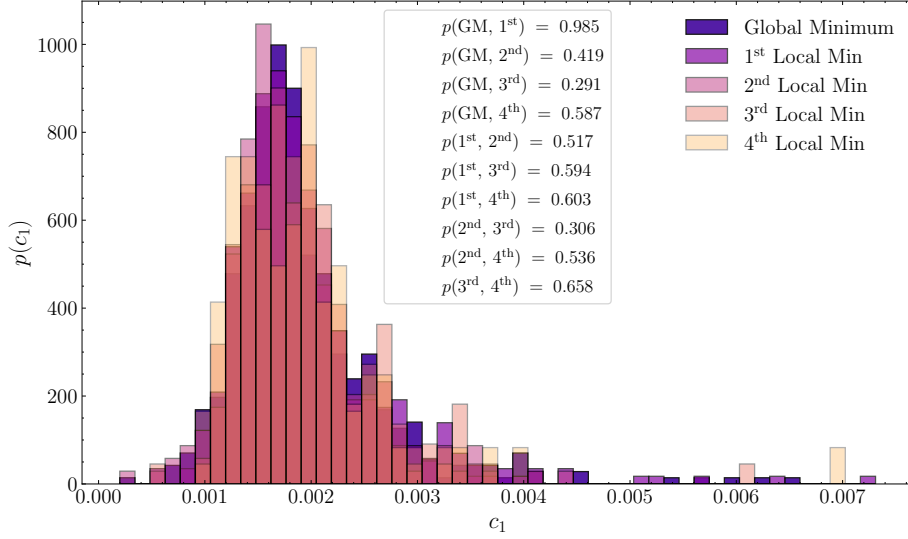


FIG. 1. Probability distributions of the leading overlap correction c_1 , defined in Eq. (21), computed on different classical minima. The distributions are sampled from 500 disorder samples for system size $L = 8$. Notice that the minima are not sampled uniformly in the classical minimization algorithm since $p_n \gg p_{n+1}$, where p_n is the probability to find the n -th minimum. In the box the p -value of the Kolmogorov-Smirnoff hypothesis test is shown for all pairs of distributions. Since the p -value is significantly greater than 0.05 for each pair, one can safely assume that c_1 is being sampled from the same distribution. Also, finding a minimum closer to the global minimum is much more likely than finding a randomly high-energy local minimum.

where $\hat{a}_i, \hat{a}_i^\dagger$ are bosonic annihilation/creation operators satisfying canonical commutation rules $[\hat{a}_i, \hat{a}_j^\dagger] = \delta_{ij}$, $[\hat{a}_i, \hat{a}_j] = [\hat{a}_i^\dagger, \hat{a}_j^\dagger] = 0$. This map preserves the spin algebra $[\hat{S}_i^\alpha, \hat{S}_j^\beta] = \delta_{ij} \epsilon_{\alpha\beta\gamma} \hat{S}_j^\gamma$, where $\alpha, \beta, \gamma = x, y, z$ and $\hat{S}^\pm = \hat{S}^x \pm i\hat{S}^y$.

In the limit of large spin S we obtain, at leading order,

$$\hat{S}_i^z \sim S - \hat{a}_i^\dagger \hat{a}_i, \quad \hat{S}_i^y \sim -i\sqrt{\frac{S}{2}}(\hat{a}_i - \hat{a}_i^\dagger), \quad \hat{S}_i^x \sim \sqrt{\frac{S}{2}}(\hat{a}_i + \hat{a}_i^\dagger). \quad (3)$$

This transformation has an intuitive interpretation: when we apply the HP map to study the quantum fluctuations around the classical ground state, the operators a, a^\dagger generate excitations in the plane orthogonal to the classical direction. The number of particle operator $\hat{n}_i \equiv \hat{a}_i^\dagger \hat{a}_i$ measures the deviation from the classical spin due to quantum fluctuation and the corresponding amplitude of fluctuation in the orthogonal plane. These excitations are quantized according to the possible values of the spin in the representation S of the $SU(2)$ group.

Disordered Holstein-Primakoff

In the case where the classical ground state is spin-glass-like, or in general a state that is not invariant under any lattice symmetry (as instead a Neél state or a ferromagnetically ordered state), building the HP Hamiltonian is not straightforward.

Consider a minimum energy configuration \mathbf{S} of the $d = 2$ disordered Heisenberg model, defined by Eq. (1). We perform a local change of reference and rewrite the classical Hamiltonian as

$$E_{cl} = \sum_{ij} J_{ij} R_i^{\beta\alpha} R_j^{t,\alpha\gamma} \Sigma_i^\beta \Sigma_j^\gamma, \quad (4)$$

where $R^{\alpha\beta} S^\beta = \Sigma^\alpha$ and $\Sigma^\alpha = \hat{z}$, so that the rotated spins Σ are all aligned along the z -axis, as would have been the case for a ferromagnetic ground state. Let us also introduce the shorthand notation $\mathcal{R}_{ij}^{\alpha\beta} \equiv R_i^{\alpha\gamma} R_j^{t,\gamma\beta}$, where the superscript t denotes matrix transposition and summation over repeated indices is implicit.

We can now apply the HP transformation at leading order to the coordinated vectors Σ : computing all the components, and promoting the classical variables Σ to quantum operators $\hat{\Sigma}$ we obtain the following identities:

$$\begin{aligned} \hat{\Sigma}_i^x \hat{\Sigma}_j^x &= \frac{1}{2S} (\hat{a}_i + \hat{a}_i^\dagger)(\hat{a}_j + \hat{a}_j^\dagger) & \hat{\Sigma}_i^y \hat{\Sigma}_j^y &= -\frac{1}{2S} (\hat{a}_i - \hat{a}_i^\dagger)(\hat{a}_j - \hat{a}_j^\dagger) \\ \hat{\Sigma}_i^z \hat{\Sigma}_j^z &= 1 - \frac{1}{S} (\hat{a}_i^\dagger \hat{a}_i + \hat{a}_j^\dagger \hat{a}_j) & \hat{\Sigma}_i^x \hat{\Sigma}_j^y &= -i \frac{1}{2S} (\hat{a}_i + \hat{a}_i^\dagger)(\hat{a}_j - \hat{a}_j^\dagger) \\ \hat{\Sigma}_i^y \hat{\Sigma}_j^z &= -i \frac{1}{\sqrt{2S}} (\hat{a}_i - \hat{a}_i^\dagger) & \hat{\Sigma}_i^x \hat{\Sigma}_j^z &= \frac{1}{\sqrt{2S}} (\hat{a}_i + \hat{a}_i^\dagger) \end{aligned} \quad (5)$$

Three different terms in the tensor $\Sigma_{ij}^{\alpha\beta}$ can be recognized: $\Sigma_{ij}^{\alpha\beta} = \Sigma_{ij}^{(0),\alpha\beta} + \Sigma_{ij}^{(1),\alpha\beta} + \Sigma_{ij}^{(2),\alpha\beta}$, where the first one contains only $O(1)$ terms and gives the classical energy, the second one contains linear terms that will vanish, since we are expanding around a minimum, and the third one is the quadratic Hamiltonian of the spin waves. From now on we focus on the latter, dropping the index $\Sigma^{(2)}$.

The Hamiltonian takes the generic form

$$\hat{H}_{SW} = \sum_{ij} \hat{a}_i^\dagger A_{ij} \hat{a}_j + \frac{1}{2} \sum_{ij} \left(\hat{a}_i^\dagger B_{ij} \hat{a}_j^\dagger + \hat{a}_i B_{ij}^* \hat{a}_j \right). \quad (6)$$

This expression can be rearranged in a more compact form by introducing the $2n$ dimensional vector $\hat{\alpha} = (\hat{a}_1, \dots, \hat{a}_n, \hat{a}_1^\dagger, \dots, \hat{a}_n^\dagger)^t$, and its adjoint $\hat{\alpha}^\dagger \gamma = \hat{\alpha}$, where $\gamma = \begin{bmatrix} 0 & 1_n \\ 1_n & 0 \end{bmatrix}$. We introduce the $2n \times 2n$ coefficients matrix $M = \begin{bmatrix} A & B \\ B^* & A^* \end{bmatrix}$ in terms of which we can express the Hamiltonian as

$$\hat{H}_{SW} = \frac{1}{2} \hat{\alpha}^\dagger M \hat{\alpha} - \frac{1}{2} \text{tr} A. \quad (7)$$

Now considering Eqs. (3) and (5) we find an expression for the matrix elements of the Hamiltonian. For $i \neq j$

$$A_{ij} = J_{ij} \mathcal{A}_{ij} = \frac{J_{ij}}{2} (\mathcal{R}_{ij}^{11} + \mathcal{R}_{ij}^{22}) + \frac{iJ_{ij}}{2} (\mathcal{R}_{ij}^{21} - \mathcal{R}_{ij}^{12}) \quad (8a)$$

$$B_{ij} = J_{ij} \mathcal{B}_{ij} = \frac{J_{ij}}{2} (\mathcal{R}_{ij}^{11} - \mathcal{R}_{ij}^{22}) + \frac{iJ_{ij}}{2} (\mathcal{R}_{ij}^{21} + \mathcal{R}_{ij}^{12}). \quad (8b)$$

For the diagonal elements we have

$$A_{ii} = - \sum_{j \in \partial i} J_{ij} \mathcal{R}_{ij}^{33}, \quad B_{ii} = 0. \quad (9)$$

By introducing the unit vector \hat{S}_{cl}^i and a pair of orthogonal unit vectors $\hat{S}_{cl}^{i,x}, \hat{S}_{cl}^{i,y}$ the matrix elements can be rewritten as

$$\mathcal{A}_{ij} = \frac{1}{2} (\hat{S}_{cl}^{i,x} - i \hat{S}_{cl}^{i,y}) (\hat{S}_{cl}^{j,x} + i \hat{S}_{cl}^{j,y}) \quad (10a)$$

$$\mathcal{B}_{ij} = \frac{1}{2} (\hat{S}_{cl}^{i,x} + i \hat{S}_{cl}^{i,y}) (\hat{S}_{cl}^{j,x} + i \hat{S}_{cl}^{j,y}). \quad (10b)$$

Notice that the theory is invariant under the local $U(1)$ transformation:

$$a_i \rightarrow e^{-i\theta_i} \quad (\hat{S}_{cl}^{i,x}, \hat{S}_{cl}^{i,y}) \rightarrow R(\theta) (\hat{S}_{cl}^{i,x}, \hat{S}_{cl}^{i,y}) \quad (11)$$

where $R(\theta)$ is the rotation matrix in the complex plane x, y . This shows that in the theory there is the freedom of choosing a local coordinate frame in the plane orthogonal to the direction fixed by the classical solution. The physical intuition is that the HP approximation describes a collection of quantum harmonic oscillators, each rotating in the plane orthogonal to the classical direction: we aim at studying the collective excitations of this system.

BOGOLJUBOV THEORY

The quadratic Hamiltonian defined in Eq. (6), for some matrices A and B , corresponds to completely generic non-interacting problem, in which both translational invariance and particle number conservation are absent. To solve the problem, one needs to find a linear transformation $T \in M_{2n \times 2n}(\mathbb{C})$, not unitary in general, which diagonalizes the quadratic form M , while preserving the bosonic commutation rules on the quasiparticle operators $\beta = T\alpha$, where $\beta^t = (\beta_1, \dots, \beta_n, \beta_1^\dagger, \dots, \beta_n^\dagger)$. This procedure is known as generalized Bogoljubov transformation [6–9].

The bosonic commutation relations for the Bogoljubov quasiparticles β can be written as

$$[\beta, \beta^\dagger] = \eta, \quad (12)$$

where η is the $2n$ dimensional metric form $\text{diag}(1, 1, \dots, -1, -1, \dots)$. This implies that the matrix T must satisfy

$$T\eta\gamma T^t = \eta\gamma, \quad (13)$$

meaning that T is an element of the symplectic group $SP(2n, \mathbb{C})$. The requirement of unitarity $T = \gamma T^* \gamma$, gives

$$T\eta T^\dagger \eta = 1. \quad (14)$$

The last equation can be used to write down an explicit form for the matrix T and its inverse

$$T = \begin{bmatrix} X^* & -Y^* \\ -Y & X \end{bmatrix} \quad T^{-1} = \begin{bmatrix} X^t & Y^\dagger \\ Y^t & X^\dagger \end{bmatrix}. \quad (15)$$

From the previous expressions, a more explicit form of the canonicity conditions can be derived, which are the straightforward generalization of the translational invariant case [6].

$$\begin{aligned} XX^\dagger - YY^\dagger &= 1_n & X^\dagger X - Y^t Y^* &= 1_n \\ XY^t - YX^t &= 0_n & X^t Y^* - Y^\dagger X &= 0_n \end{aligned} \quad (16)$$

Plugging in Eq. (7) the definition of the Bogoljubov transformation, one finds

$$\hat{H}_{SW} = \frac{1}{2}\beta^\dagger \eta T \eta M T^{-1} \beta - \frac{1}{2}\text{tr} A \quad (17)$$

Therefore, the solution of the problem reduces to finding the eigenvalues and eigenvectors of the non-Hermitian matrix ηM , also called dynamical matrix [10]. It is possible to show that if the matrix M is positive definite, the spectrum of ηM is real [8]. This is the physically relevant case, since the spin wave Hamiltonian is obtained by expanding around a minimum.

The matrix ηM is not hermitian, so it is not guaranteed that the algebraic dimension of a degenerate eigenspace — the number of degenerate eigenvalues — is equal to the geometric dimension of such eigenspace — the number of linearly independent eigenvectors. If this happens, it is not possible to define anymore the inverse as in Eq. (15). In a disordered system, typically there are no degenerate finite eigenvalues, but in the system defined in Eq. (6) there are zero modes associated to global spin rotations (i.e. Goldstone modes). To avoid dealing with this problem, we added to the Hamiltonian a symmetry breaking field on the first two sites, that completely removes the degeneracy eliminating the degenerate kernel of the matrix ηM . We performed a careful study of the dependence on the external field, showing that this procedure is solid and extrapolates to the correct result when the strength of the field is sent to zero.

Two point correlation function and the order parameter quantum correction.

We are interested in the computation of the quantum corrections to the 2-point correlation function squared, at leading order $1/S$:

$$\begin{aligned} \langle \hat{\mathbf{S}}_i \cdot \hat{\mathbf{S}}_j \rangle^2 &= \left(\langle \mathbf{S}_i \cdot \mathbf{S}_j \rangle_{CL} + \frac{1}{S} \left(\langle \mathbf{S}_i \delta \hat{\mathbf{S}}_j \rangle + \langle \mathbf{S}_j \delta \hat{\mathbf{S}}_i \rangle \right) + \frac{1}{S} \langle \delta \hat{\mathbf{S}}_i \cdot \delta \hat{\mathbf{S}}_j \rangle_0 + \dots \right)^2 = \\ &= \langle \mathbf{S}_i \cdot \mathbf{S}_j \rangle_{CL}^2 + \frac{2}{S} \langle \mathbf{S}_i \cdot \mathbf{S}_j \rangle_{CL} \left(\mathcal{R}_{ij}^{zz} \left(\langle \Sigma_i^z \delta \hat{\Sigma}_j^z \rangle + \langle \Sigma_j^z \delta \hat{\Sigma}_i^z \rangle \right) + \mathcal{R}_{ij}^{\alpha\beta} \langle \delta \hat{\Sigma}_i^\alpha \delta \hat{\Sigma}_j^\beta \rangle \right), \end{aligned} \quad (18)$$

where $\alpha, \beta = x, y$ and $\langle \cdot \rangle = \langle 0 | \cdot | 0 \rangle$ stands for the Bogoljubov vacuum state average. By using the HP representation, we find that the quantum fluctuation correlation function reads

$$\langle \delta \hat{\mathbf{S}}_i \cdot \delta \hat{\mathbf{S}}_j \rangle = \langle \hat{a}_i^\dagger \hat{a}_j \rangle \mathcal{A}_{ij} + \langle \hat{a}_i \hat{a}_j^\dagger \rangle \mathcal{A}_{ij}^* + \langle \hat{a}_i^\dagger \hat{a}_j^\dagger \rangle \mathcal{B}_{ij} + \langle \hat{a}_i \hat{a}_j \rangle \mathcal{B}_{ij}^* \quad (19a)$$

$$\langle \mathbf{S}_i \cdot \delta \hat{\mathbf{S}}_j \rangle = -\langle \hat{a}_j^\dagger \hat{a}_j \rangle \mathcal{R}_{ij}^{33}. \quad (19b)$$

We need to evaluate the expectation values of the creation/annihilation operators on the ground state of the quantum theory. By exploiting the definition of the inverse transformation in Eq. (15) we find

$$\begin{aligned} \langle \hat{a}_i^\dagger \hat{a}_j \rangle &= (Y^t Y^*)_{ij} & \langle \hat{a}_i \hat{a}_j^\dagger \rangle &= (X^t X^*)_{ij} \\ \langle \hat{a}_i \hat{a}_j \rangle &= (X^t Y^*)_{ij} & \langle \hat{a}_i^\dagger \hat{a}_j^\dagger \rangle &= (Y^t X^*)_{ij}. \end{aligned} \quad (20)$$

These are the only surviving terms, since in the inverse Bogoljubov transformation the only nonzero contributions come from $\langle \hat{b}\hat{b}^\dagger \rangle$.

We find that the correlation function decays exponentially with distance. The lack of long range order is due to the random structure of the correlation function, where the expectation values of bosonic operators are multiplied by random coefficients coming from the classical solution. From the correlation function, it is possible to compute the first correction to the classical order parameter:

$$c_1 = \frac{1}{L^4} \sum_{ij} C_{ij} = \frac{1}{L^4} \sum_{ij} \mathcal{R}_{ij}^{zz} \left(\langle \Sigma_i^z \delta \hat{\Sigma}_j^z \rangle + \langle \Sigma_j^z \delta \hat{\Sigma}_i^z \rangle \right) + \mathcal{R}_{ij}^{\alpha\beta} \langle \delta \hat{\Sigma}_i^\alpha \delta \hat{\Sigma}_j^\beta \rangle, \quad (21)$$

where C_{ij} is defined implicitly, referring to Eq. (18). As we show in the paper, c_1 vanishes in the thermodynamic limit, indicating the very plausible presence of a critical value of the spin representation until which the SG order is maintained.

-
- [1] N. Dupuis, *Field Theory of Condensed Matter and Ultracold Gases* (World Scientific, 2023).
 - [2] M. Baity-Jesi, V. Martín-Mayor, G. Parisi, and S. Perez-Gaviro, *Phys. Rev. Lett.* **115**, 267205 (2015).
 - [3] H. Kawamura and H. Yonehara, *Journal of Physics A: Mathematical and General* **36**, 10867 (2003).
 - [4] J. F. Fernandez, *Journal of Physics C: Solid State Physics* **10**, L441 (1977).
 - [5] M. Baity-Jesi and G. Parisi, *Physical Review B* **91**, 134203 (2015).
 - [6] N. N. Bogoljubov, *Journal of Physics (USSR)* **11**, 23 (1947).
 - [7] A. L. Fetter and J. D. Walecka, *Quantum Theory of Many-Particle Systems* (Dover Publications, 2003).
 - [8] J.-P. Blaizot and G. Ripka, *Quantum Theory of Finite Systems* (MIT Press, Cambridge, Massachusetts, 1986).
 - [9] J. Colpa, *Physica A: Statistical Mechanics and its Applications* **93**, 327 (1978).
 - [10] M.-W. Xiao, *Theory of transformation for the diagonalization of quadratic hamiltonians* (2009), [arXiv:0908.0787 \[math-ph\]](https://arxiv.org/abs/0908.0787).